machines

MDPI

Article

Research on Pressure Control of Hydraulic System for Pump Controlled Anchor Drilling Machine Based on Variable Universe Fuzzy PID Algorithm

Zheng Yan [1,*], Guangwei Tang [2] and Youshan Gao [2]

[1] Department of Mechanics, Jinzhong University, Jinzhong 030619, China
[2] School of Mechanical Engineering, Taiyuan University of Science and Technology, Taiyuan 030024, China; tgw28@foxmail.com (G.T.); gaoyoushan@tyust.edu.cn (Y.G.)
* Correspondence: yanz79@126.com

Abstract: To address significant pressure fluctuations in anchor drilling machine systems during the drilling and anchoring support of complex coal roadway surrounding rock, a variable universe fuzzy PID control strategy was proposed to regulate the speed of the servo motor. Additionally, a pump-controlled pressure approach was introduced to further reduce throttling losses and energy consumption. To validate the proposed algorithm, disturbances were simulated by adjusting the opening size of a three-position four-way proportional directional valve. A co-simulation model was first established using AMESIM 2020.1 and SIMULINK R2022a software, followed by experimental verification and comparison with conventional PID control. The experimental results demonstrated that when the system pressure signal was set to a constant value, the proposed algorithm reduced the pressure error by approximately 36.5% compared to PID control. For step pressure inputs, the algorithm decreased the response time and overshoot by 6.8–8.2% and 10.3–16.2%, respectively, under different valve openings. Furthermore, when the system pressure followed various sinusoidal signals, the proposed algorithm exhibited lower pressure error and faster response times than PID control. This study provides theoretical and experimental references for maintaining stable pressure during the operation of anchor drilling machines, offering an efficient and reliable control solution for complex drilling environments.

Keywords: asynchronous servomotor; pump control; variable universe fuzzy PID; system pressure control; anchor drilling machine

check for updates

Academic Editor: Zheng Chen

Received: 5 February 2025
Revised: 21 February 2025
Accepted: 25 February 2025
Published: 28 February 2025

Citation: Yan, Z.; Tang, G.; Gao, Y. Research on Pressure Control of Hydraulic System for Pump Controlled Anchor Drilling Machine Based on Variable Universe Fuzzy PID Algorithm. *Machines* **2025**, *13*, 199. https://doi.org/10.3390/machines13030199

Copyright: © 2025 by the authors. Licensee MDPI, Basel, Switzerland. This article is an open access article distributed under the terms and conditions of the Creative Commons Attribution (CC BY) license (https://creativecommons.org/licenses/by/4.0/).

1. Introduction

Anchor drilling rigs are specialized equipment used in anchor support operations to drill anchor holes, install anchors, and secure them [1,2]. These rigs inherently exhibit nonlinear and time-varying parameter characteristics. The complex and variable nature of the surrounding rock conditions leads to nonlinear loading. Currently, tunnel support operations remain largely dependent on manual labor, and the hydraulic systems demonstrate time delays. Consequently, the fluctuating surrounding rock conditions cause significant pressure variations within the drilling rig system, which not only affect the service life of hydraulic components but also prevent the system from rapidly adapting to load changes. This results in frequent occurrences of drilling jams and even rod breakage incidents.

To mitigate system pressure fluctuations, research is conducted from two primary perspectives. The first approach involves improving the design of the system's inherent

components, while the second employs high-efficiency controllers on existing components. The former can fundamentally reduce fluctuation amplitudes; however, it typically requires higher costs and longer development periods. Alternatively, designing an effective controller can similarly achieve significant improvements in system control performance.

To enable the dual-power heads of anchor drilling rigs to output independent pressure and flow, Ning Zhang et al. proposed the use of a load-independent flow distribution system [3]. Chenghu Guo developed a two-stage safety valve combining direct-acting and differential valves to stabilize system pressure [4]. Cao Chao et al. introduced a novel configuration for a servo pump-based fast pump control and pressure stabilization liquid supply system to reduce the large and frequent pressure shocks caused by hydraulic supports and machine operations [5]. To minimize pressure fluctuations in the hydraulic cylinder chambers caused by sudden changes in control signals in excavator load port independent control systems, Cheng Min et al. proposed modifying sudden control signals using a nonlinear filter [6]. Chen Yuanling et al. suggested adding an accumulator at the pump outlet of a load-sensitive pump to reduce significant hydraulic shocks caused by large amplitude loads during the operation of sugarcane combine harvesters [7]. Wei Lingtiao et al. introduced a hierarchical pressure control strategy considering coil temperature estimation, ensuring the stability and accuracy of pressure in plunger pump-based pressurization units under temperature influences [8]. Zhang Yan'an et al. developed a model-free adaptive control method based on an improved genetic algorithm to enhance the accuracy of pressure control in wet clutch transmissions of tractor power shift gearboxes [9]. Gao Qiang et al., utilizing type A half-bridge liquid resistance circuits and parallel digital hydraulic technology, proposed an array digital valve-controlled electro-hydraulic pressure servo structure to meet the high reliability requirements of electro-hydraulic pressure servo control technology in variable speed helicopter friction clutch transmissions [10]. Chen Zheng et al. proposed a load port independent control system method based on cavity pressure planning and pressure tracking to reduce pressure fluctuations caused by frequent switching of control targets in the same cavity under different modes [11]. Su Chunbo et al. decoupled and reduced the multi-dynamic coupling of pressure pulse fatigue testing systems using singular value perturbation theory and compensated for system model uncertainties with an active disturbance rejection control algorithm [12]. Ge Lei et al. addressed the challenge of adapting to rapid and random load flow changes in variable speed pressure control by proposing a pressure control scheme based on torque control and speed compensation [13]. Li Wenjing et al., based on the working principles of high-frequency solenoid valve pressure control in train electro-hydraulic braking systems, employed an adaptive fuzzy PID controller to adjust the duty cycle of PWM control signals, thereby regulating the switching actions of high-frequency solenoid valves [14]. Tan Cao et al. introduced a cascaded control method combining external loop wheel cylinder pressure control with internal loop direct-drive pump piston position control to achieve distributed braking system pressure control [15]. Xia Yimin et al., focusing on valve-controlled cylinder systems controlled by proportional relief valves and proportional speed control valves, proposed a pressure-speed composite control strategy based on a backstepping integral adaptive control algorithm [16]. Qi Zhong et al., investigating the impact of valve spool displacement characteristics on system pressure and flow control in load port independent control systems, designed pressure and flow controllers based on a two-stage fuzzy PID approach [17]. Feng Jiangtao et al., addressing significant hydraulic shocks in missile launch systems during load start-up and braking processes, designed a load port independent control system based on flow feedback and pressure closed-loop control [18]. Yu Jin et al., aiming to enhance the tracking control performance of hydraulic machinery's continuously variable transmissions, developed a variable domain fuzzy PID controller with quantization and

decision factor scaling variations [19]. Gao Youshan et al., to reduce flow pulsations and hydraulic shocks in variable displacement asymmetric pumps, analyzed the effects of distribution window B and T port connectivity and swash plate tilt angles [20].

In summary, although some scholars have made breakthroughs in developing controllers to reduce system pressure shocks, their efforts have primarily focused on valve control strategies that directly manage system pressure without further consideration of unknown disturbances' impacts on the system. Additionally, there has been limited research on pump-controlled system pressure, particularly regarding variable domain fuzzy PID control algorithms for servo motors. Electro-hydraulic power sources can provide the necessary pressure and flow for hydraulic systems [21]. Due to the higher control precision and broader power control range of servo motors compared to variable frequency asynchronous motors, they can reduce system energy consumption and adapt to load changes [22]. Therefore, this study proposes controlling the pump motor speed to regulate system pressure and introduces a variable domain fuzzy PID controller for the servo motor speed to enhance system responsiveness and anti-disturbance performance.

The remainder of this paper is organized as follows: Section 2 establishes the mathematical model of the system; Section 3 designs the controller for the proposed algorithm; Section 4 conducts co-simulations and experiments to validate the accuracy and rationality of the proposed method; and Section 5 presents the conclusions.

2. System Principles and Mathematical Model

2.1. System Operating Principles

The system architecture is illustrated in Figure 1. An asynchronous servomotor 1 drives a metering pump 2, serving as the primary power source for the entire system. System pressure is regulated by adjusting the speed of the servomotor. To validate the superior performance of the proposed algorithm, the valve opening of a three-position four-way proportional directional valve 4 is designated as a system disturbance, while the relief valve 3 functions as the system safety valve.

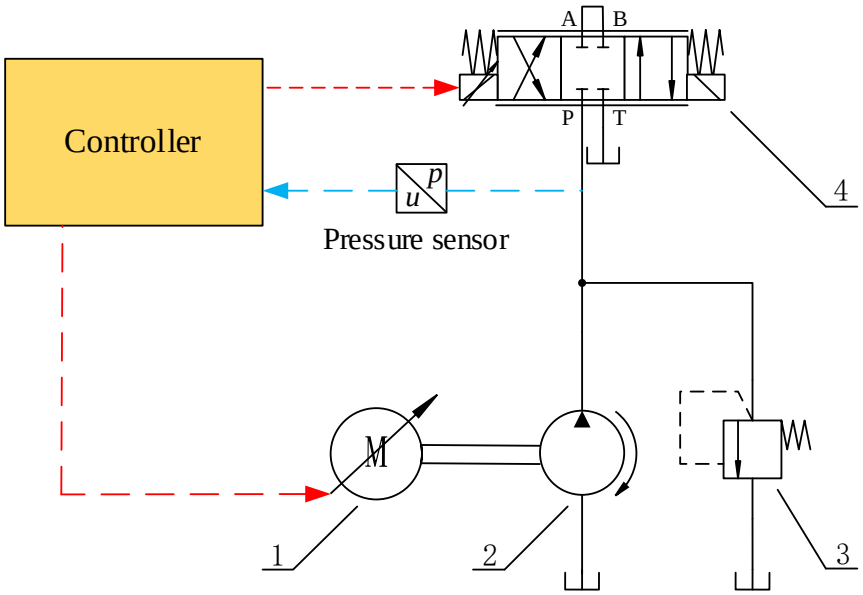


Figure 1. System architecture diagram. The red line represents the control line, the blue line represents the signal feedback line, and the black line represents the oil circuit of the hydraulic system itself.

2.2. Relevant Mathematical Models

An asynchronous servomotor is a specialized type of asynchronous motor [23,24]. Consequently, its steady-state model is identical to that of a conventional squirrel-cage

asynchronous motor. After a series of coordinate transformations, the mathematical model of the motor in the $d-q$ axis coordinate system is expressed as follows:

(1) The flux linkage equation is:

$$\begin{bmatrix} \psi_{sd} \\ \psi_{sq} \\ \psi_{rd} \\ \psi_{rq} \end{bmatrix} = \begin{bmatrix} L_s & 0 & L_m & 0 \\ 0 & L_s & 0 & L_m \\ L_m & 0 & L_r & 0 \\ 0 & L_m & 0 & L_r \end{bmatrix} \begin{bmatrix} i_{sd} \\ i_{sq} \\ i_{rd} \\ i_{rq} \end{bmatrix} \tag{1}$$

In the equation:

$i_{sd}, i_{sq}, i_{rd}, i_{rq}$ represents the current components of the motor stator and rotor along the $d-q$ axis;

L_s, L_r, L_m denotes the self-inductance of the stator and rotor as well as the mutual inductance between them;

$\psi_{sd}, \psi_{sq}, \psi_{rd}, \psi_{rq}$ represents the flux linkage components of the stator and rotor along the $d-q$ axis.

(2) The voltage equation in the rotating $d-q$ axis coordinate system is:

$$\begin{bmatrix} u_{sd} \\ u_{sq} \\ u_{rd} \\ u_{rq} \end{bmatrix} = \begin{bmatrix} R_s + L_s P & -\omega_1 L_s & L_m P & -\omega_1 L_m \\ \omega_1 L_s & R_s + L_s P & \omega_1 L_m & L_m P \\ L_m P & -\omega_s L_m & R_r + L_r P & -\omega_s L_r \\ \omega_s L_m & L_m P & \omega_s L_r & R_r + L_r P \end{bmatrix} \begin{bmatrix} i_{sd} \\ i_{sq} \\ i_{rd} \\ i_{rq} \end{bmatrix} \tag{2}$$

In the equation:

Since the rotor windings of the squirrel-cage motor are short-circuited, $u_{rd} = u_{rq} = 0$;

$u_{sd}, u_{sq}, u_{rd}, u_{rq}$ represents the voltage components of the motor along the $d-q$ axis;

R_s, R_r denotes the resistances of the motor's stator and rotor;

$\omega_s = \omega_1 - \omega_r$ represents the slip angular velocity of the motor, where ω_1 is the synchronous angular velocity and ω_r the rotor angular velocity;

$P = \frac{d}{dt}$ is the differential operator.

(3) The torque equation is:

$$T_e = p_n L_m \left(i_{sq} i_{rd} - i_{sd} i_{rq}\right) = \frac{p_n L_m \left(i_{sq} \psi_{rd} - i_{sd} \psi_{rq}\right)}{L_r} \tag{3}$$

In the equation:

P_n represents the number of pole pairs of the motor.

Let the $d-q$ coordinate system synchronize with the rotor flux vector, with the d-axis aligned with the rotor flux vector, designated as the m-axis. The q-axis is set to lead the d-axis by 90°, designated as the t-axis. This results in the rotor-flux-oriented synchronous rotating coordinate system $m-t$, as shown in Figure 2.

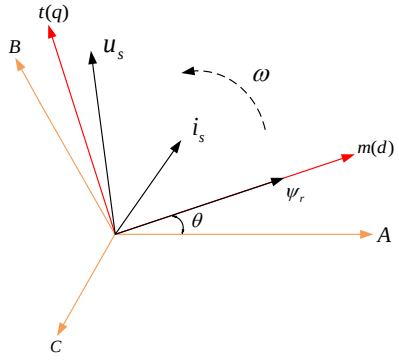


Figure 2. Rotor-Flux-Oriented synchronous rotating coordinate system (m-t).

Since the m-axis coincides with the rotor flux vector, the following can be derived:

$$\begin{cases} \psi_{rm} = \psi_{rd} = \psi_r \\ \psi_{rt} = \psi_{rq} = 0 \end{cases} \tag{4}$$

To ensure that the m-axis always remains aligned with the rotor flux vector, the following condition must be satisfied:

$$\frac{d\psi_{rt}}{dt} = \frac{d\psi_{rq}}{dt} = 0 \tag{5}$$

Thus, the state equations in the rotor-flux-oriented synchronous rotating coordinate system $m - t$ are obtained as:

$$\begin{cases} \frac{di_{sm}}{dt} = \frac{L_m}{\sigma L_s L_r T_r}\psi_r - \frac{R_s L_r^2 + R_r L_m^2}{\sigma L_s L_r^2} i_{sm} + \omega_1 i_{st} + \frac{u_{sm}}{\sigma L_s} \\ \frac{di_{st}}{dt} = -\frac{L_m \omega_r}{\sigma L_s L_r}\psi_r - \frac{R_s L_r^2 + R_r L_m^2}{\sigma L_s L_r^2} i_{st} - \omega_1 i_{sm} + \frac{u_{st}}{\sigma L_s} \end{cases} \tag{6}$$

The difference between the angular velocity of the rotating coordinate system and the rotor speed is defined as the slip angular frequency ω_s:

$$\omega_s = \frac{L_m}{T_r \psi_r} i_{st} \tag{7}$$

In the equation:

L_m represents the mutual inductance between the stator and rotor of the motor.

T_r represents the rotor time constant, $T_r = L_r / R_r$;

ψ_r represents the rotor flux linkage, $\psi_r = L_m i_{sm} / (T_r P + 1)$;

σ represents the leakage coefficient, $\sigma = 1 - L_m^2 / (L_s L_r)$;

i_{sm} represents the magnetizing component of the stator current along the m-axis;

i_{st} represents the torque-producing component of the stator current along the t-axis.

The new electromagnetic torque expression, based on rotor flux orientation, can be derived as:

$$\begin{aligned} T_e &= p_n L_m \left(i_{sq} i_{rd} - i_{sd} i_{rq}\right) = \frac{p_n L_m \left(i_{sq}\psi_{rd} - i_{sd}\psi_{rq}\right)}{L_r} \\ &= \frac{p_n L_m}{L_r} i_{st} \psi_r \end{aligned} \tag{8}$$

(4) The motor load torque formula is:

$$T_L = \frac{P_s D_p}{\eta_{pm}} \tag{9}$$

In the equation:

T_L represents the output torque of the variable pump, which is also referred to as the load torque, $T_L = T_p$;

P_s represents the output pressure of the variable pump;

D_p represents the displacement of the variable pump;

η_{pm} represents the mechanical efficiency of the variable pump, which can be taken as 0.95.

(5) The mechanical motion equation is:

$$T_e - T_L = \frac{J_m}{p_n}\frac{d\omega_r}{dt} + \frac{B\omega_r}{p_n} \tag{10}$$

In the equation:

J_m represents the rotational inertia (moment of inertia) of the motor;

B represents the viscous friction coefficient of the motor;

ω_r represents the rotational speed of the motor rotor.
Here, ω_r represents the electrical angular velocity, expressed as: $\omega_r = p_n\omega_m$.
(6) Three-position four-way proportional directional control valve:
Since no actuator or other load is applied, $p_1 = p_2 = p_L$.

$$Q_L = K_q x_v \tag{11}$$

In the equation:
K_q represents the flow gain of the valve. x_v represents the motion displacement of the valve.

3. The Design of the Controller

3.1. Fuzzy PID Controller Section

The controller designed in this study adopts a two-input and three-output structural configuration. The input variables of the controller are defined as the pressure error e of the propulsion system and the rate of change of the error ec. Through fuzzy control, the three tuning parameters of the PID controller (Δk_p, Δk_i, and Δk_d) are adjusted. The expression for the fuzzy PID control parameters is as follows:

$$\begin{cases} K_p = K_{p0} + \Delta k_p \cdot k_p \\ K_i = K_{i0} + \Delta k_i \cdot k_i \\ K_d = K_{d0} + \Delta k_d \cdot k_d \end{cases} \tag{12}$$

In the equation:
k_p, k_i and k_d represent the correction factor coefficients. K_{p0}, K_{i0} and K_{d0} represent the initial parameters of the PID controller.

The input and output variable universes of discourse are proportionally divided into seven fuzzy subsets: PB (Positive Big), PM (Positive Medium), PS (Positive Small), ZO (Zero), NS (Negative Small), NM (Negative Medium), and NB (Negative Big). Considering the range of pressure variations in the experimental system, the basic universes of discourse for the error e and the rate of change of the error ec are defined as $[-3, 3][-3, 3][-3, 3]$, and $[-2.5, 2.5][-2.5, 2.5][-2.5, 2.5]$, respectively, while the basic universes of discourse for Δk_p, Δk_i and Δk_d are all defined as $[-1, 1][-1, 1][-1, 1]$. The basic universes of discourse and the fuzzy universes of discourse are mapped by adjusting the proportional and quantization factors to achieve better control performance. Given the need for high sensitivity in nonlinear system control, triangular membership functions are adopted for the input and output of all variables in the controller.

The rational design of fuzzy control rules is the core of the entire controller, with the fundamental objective of minimizing errors and maintaining system stability. The fuzzy inference process relies on the fuzzy rule table, where input fuzzy variables are mapped to different membership functions depending on their respective universes of discourse. Through the application of fuzzy rules, different output fuzzy variables are generated. Accordingly, the fuzzy control rules are formulated as shown in Table 1.

The fuzzification of the input variables in this study adopts the Mamdani method (also known as the truncation method). The universe of discourse for each variable is defined and then discretized to form a discrete set. Fuzzification of precise values is achieved through the use of membership functions. Consequently, the centroid method is selected for defuzzification of the fuzzy variables. The calculation formula is as follows:

$$u = \frac{\sum_{i=1}^{n} x_i A(e_i, ec_i)}{\sum_{i=1}^{n} A(e_i, ec_i)} \tag{13}$$

In the equation:
x_i represents an element of the fuzzy subset u;
$A(e_i, ec_i)$ represents the corresponding membership function.

Table 1. Fuzzy rule control table.

ΔK_p		ec						
Δk_i	Δk_d	NB	NM	NS	ZO	PS	PM	PB
e	NB	$PB/NB/PS$	$PB/NB/NS$	$PM/NM/NB$	$PM/NM/NB$	$PS/NS/NB$	$ZO/ZO/NM$	$ZO/ZO/NS$
	NM	$PB/NB/PS$	$PB/NB/NS$	$PM/NM/NB$	$PS/NS/NM$	$PS/NS/NM$	$ZO/ZO/NS$	$NS/ZO/ZO$
	NS	$PM/NB/ZO$	$PM/NM/NS$	$PM/NS/NM$	$PS/NS/NM$	$ZO/ZO/NS$	$NS/PS/NS$	$NS/PS/ZO$
	ZO	$PM/NM/ZO$	$PM/NM/NS$	$PS/NS/NS$	$ZO/ZO/NS$	$NS/PS/NS$	$NM/PM/NS$	$NM/PM/ZO$
	PS	$PS/NM/ZO$	$PS/NS/ZO$	$ZO/ZO/ZO$	$NS/PS/ZO$	$NS/PS/ZO$	$NM/PM/ZO$	$NM/PB/ZO$
	PM	$PS/ZO/PB$	$ZO/ZO/NS$	$NS/PS/PS$	$NM/PS/PS$	$NM/PM/PS$	$NM/PB/PS$	$NB/PB/PB$
	PB	$ZO/ZO/PB$	$ZO/ZO/PM$	$NM/PS/PM$	$NM/PM/PM$	$NM/PM/PS$	$NB/PB/PS$	$NB/PB/PB$

3.2. Design of the Variable Universe Fuzzy PID Controller

The variable universe fuzzy PID control is a novel approach that combines the concept of variable universes with fuzzy PID control [25,26]. The universe of discourse is adjusted in real time according to changes in the input. The corresponding rules are as follows: when the error is large, the adaptive scaling factor enlarges the fuzzy universe, thereby extending the associated membership functions and reducing the redundancy of fuzzy rules. Conversely, when the error is small, the fuzzy universe is reduced, and the associated membership functions are compressed, effectively increasing the number of fuzzy rules, as illustrated in Figure 3. This mechanism helps to prevent system oscillations and poor disturbance rejection caused by input variations, thereby ensuring system stability.

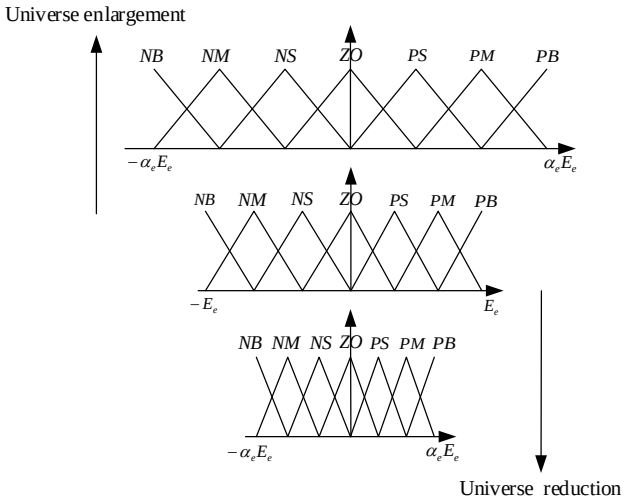


Figure 3. Variable universe scaling diagram.

Therefore, the initial universes of discourse are set as $X_e = [-E_e, E_e]$, $X_{ec} = [-E_{ec}, E_{ec}]$, and $U_c = [-U, U]$. After adjustment through the introduction of scaling factors, the fuzzy universes of discourse are expressed as [27]:

$$\begin{cases} X_e = [-\alpha_e E_e, \alpha_e E_e] \\ X_{ec} = [-\alpha_{ec} E_{ec}, \alpha_{ec} E_{ec}] \\ U_c = [-\beta U, \beta U] \end{cases} \tag{14}$$

Since the function-based scaling factor is constant, it requires a manual selection of appropriate parameters to achieve the desired control effect [28–30]. Therefore, this study adopts scaling factors based on fuzzy rules. The scaling factors for the universes of

discourse of error e and error rate of change ec are denoted as α_e and α_{ec}, respectively. Their value ranges are set to [0.5, 6.5][0.5, 6.5][0.5, 6.5] for α_e and [0.4, 1][0.4, 1][0.4, 1] for α_{ec}. α_e and α_{ec} are divided into four fuzzy levels, expressed in fuzzy linguistic terms as "amplify", "moderately amplify", "slightly amplify", and "no amplification", corresponding to the fuzzy subset $\{B, M, S, ZO\}$. The rules are provided in Table 2.

Table 2. Fuzzy Rule Table for Scaling Factors α_e and α_{ec}.

$e(t)$	NB	NM	NS	ZO	PS	PM	PB
α_e	B	M	S	ZO	S	M	B
$ec(t)$	NB	NM	NS	ZO	PS	PM	PB
α_{ec}	B	M	S	ZO	S	M	B

The scaling factor β of the output variable domain is similarly determined jointly by e and ec, with its domain defined as [0.3, 0.9][0.3, 0.9][0.3, 0.9]. To enhance control accuracy, the domain is divided into seven fuzzy linguistic levels: super large, positive large, positive medium, medium-small, positive small, super small, and zero, corresponding to the fuzzy subsets $\{VB, B, M, MS, S, VS, ZO\}$. When both e and ec are large and have the same sign, this indicates that the deviation between the actual system pressure and the setpoint is significant. In such cases, the output domain needs to be expanded to ensure the system pressure reaches the target setpoint. Conversely, when e and ec are large but have opposite signs, this suggests a significant deviation between the actual system pressure and the target value, but the system is recovering rapidly toward the setpoint. Under these conditions, the domain should remain unchanged. When e is small and ec is large with the same sign, this indicates that the actual system pressure is gradually moving away from the setpoint, requiring an appropriate expansion of the domain. The specific fuzzy rules for the scaling factor are presented in Table 3.

The structural principle of the controller is shown in Figure 4.

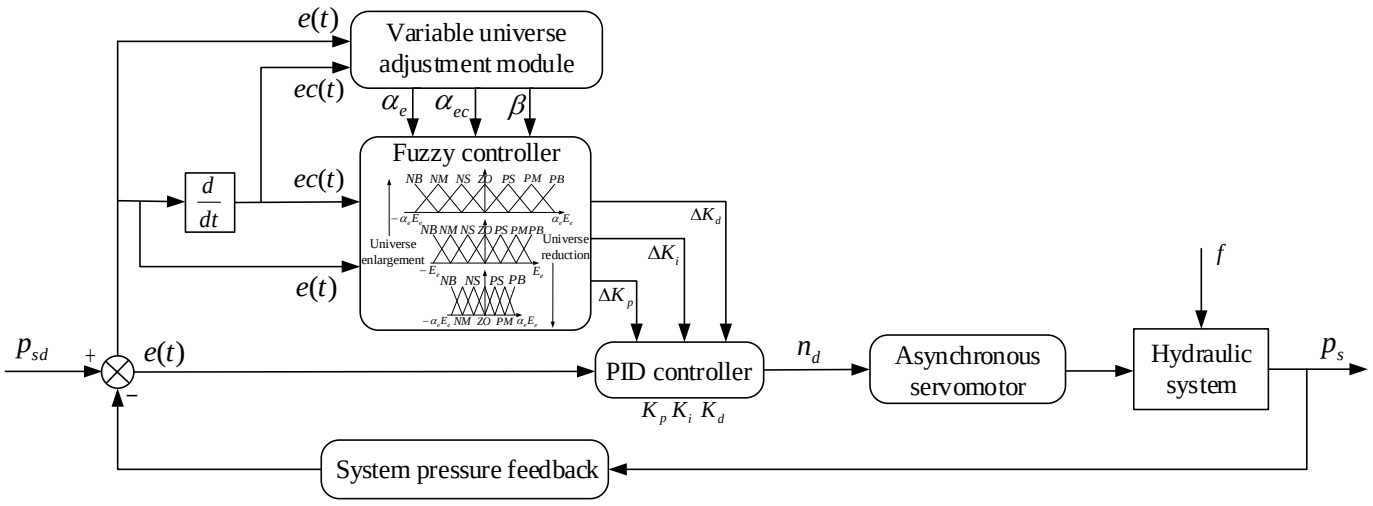


Figure 4. Diagram of the system controller structural principle.

In summary, the output signal of the variable domain fuzzy PID controller can be expressed as:

$$u(t) = (K_{p0} + \Delta K_p)e(t) + (K_{i0} + \Delta K_i)\int e(t)dt + (K_{d0} + \Delta K_d) \cdot \frac{de(t)}{dt} \tag{15}$$

In the equation:

ΔK_p, ΔK_i and ΔK_d are the parameters adjusted through variable domain fuzzy control.

Table 3. Fuzzy Rule Table for the Scaling Factor β.

β		$ec(t)$						
		NB	NM	NS	ZO	PS	PM	PB
$e(t)$	NB	VB	VB	VB	B	MS	S	ZO
	NM	VB	VB	B	B	MB	S	VS
	NS	VB	MB	B	VB	VS	S	VS
	ZO	S	MS	MB	ZO	MB	MS	S
	PS	VS	S	VS	VB	B	MB	VB
	PM	VS	S	MB	B	B	VB	VB
	PB	ZO	S	MS	B	VB	VB	VB

4. Simulation and Experimental Validation

In this section, the results of combined simulation and experimental analysis are presented. The system pressure is set under three different operating conditions: a constant value, a step change, and a sinusoidal variation. The performance of the proposed algorithm is investigated and compared to that of traditional PID control under these conditions.

4.1. Combined Simulation

In this study, the simulation model was constructed using AMESIM and MATLAB/Simulink. The hydraulic subsystem was modeled in AMESIM, while the motor model was developed in Simulink. The parameters for system simulation and modeling are listed in Table 4.

Table 4. System simulation parameters.

Parameter	Value
Motor power (KW)	30
Power Factor (cosφ)	0.83
Mechanical Efficiency	0.941
Rated Torque (N·m)	108
Displacement of Fixed Displacement Pump (mL/r)	13.5
Input Signal of Proportional Directional Valve (mA)	±10
Valve Port Pressure Difference (MPa)	1
Relief Valve Pressure (MPa)	16

Similarly, the controller algorithm is also implemented in Simulink, and its schematic diagram is shown in Figure 5.

During the drilling and anchoring support operations of a bolting rig, various complex surrounding rock conditions are encountered. The presence of rock debris or even cracks can lead to significant fluctuations in drilling pressure. To simulate these conditions, three scenarios were defined: drilling with a constant system pressure of 4 MPa, step changes in system pressure to 6 MPa during drilling when the hardness of the coal seam surrounding rock increases sharply, and sinusoidal variations in system pressure at 8 ± 1 MPa to approximate the uneven thickness of the surrounding rock in the coal seam.

As shown in Figure 6, when the system pressure is set to a constant value of 4 MPa for drilling, and the input current of the proportional directional valve is adjusted to 3.4 ± 0.1 mA with a 1 Hz sinusoidal signal as the pressure disturbance, the PID control results in significant pressure fluctuations. However, under the proposed algorithm, the pressure error is reduced by 37.8%.

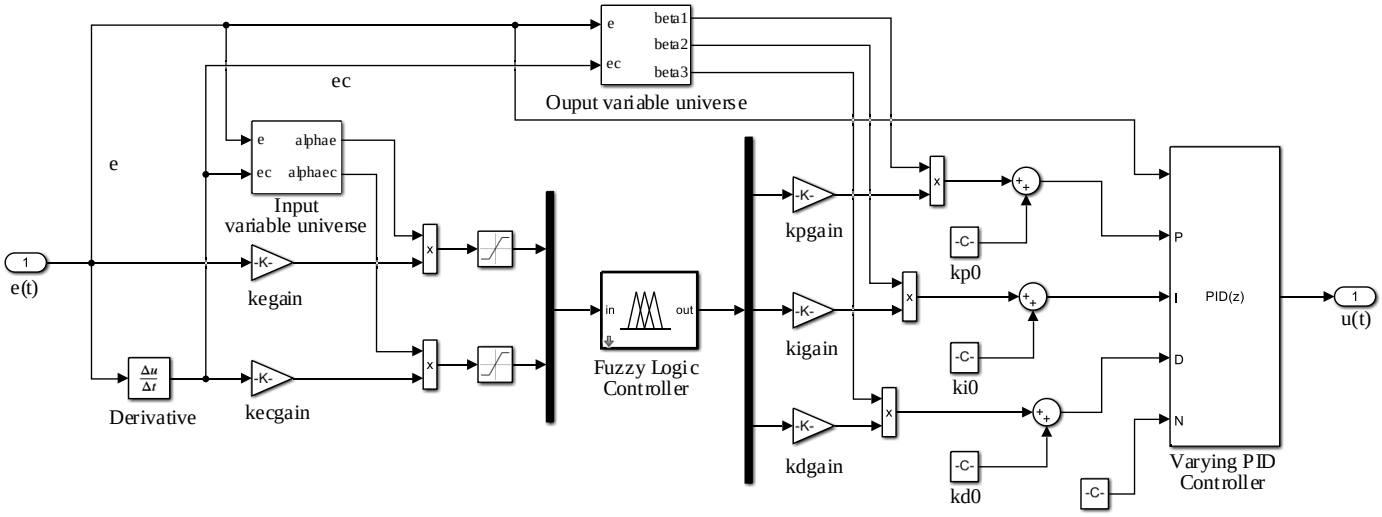
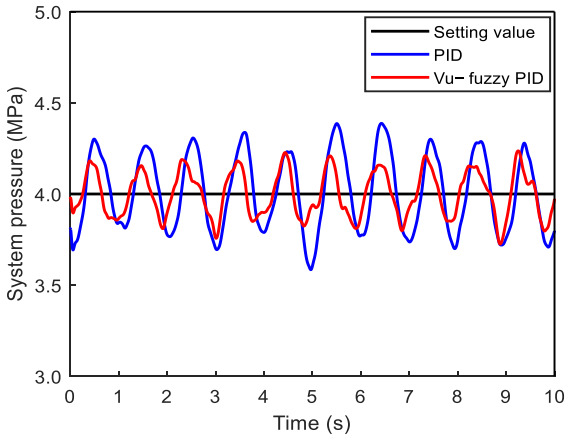
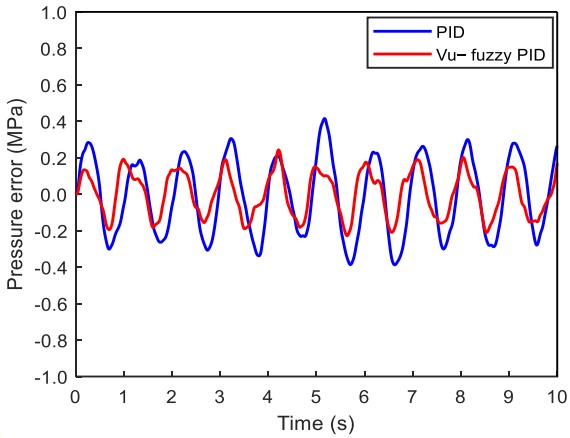


Figure 5. Schematic diagram of variable universe fuzzy PID control.



(**a**) Pressure Tracking Performance



(**b**) Pressure Error Variation

Figure 6. Simulation of 4 MPa Constant System Pressure.

As shown in Figure 7, when the system pressure steps from 0 MPa to 6 MPa, with the proportional directional valve input current set to 3.4 ± 0.1 mA and a 1.5 Hz sinusoidal signal as the disturbance, the proposed control algorithm reduces the response time by 7.4% and the overshoot by 18.1% compared to PID control. Additionally, when the disturbance signal is set to 3.4 ± 0.2 mA and 1 Hz as the input current of the proportional directional valve, the proposed algorithm achieves reductions in overshoot and response time of 11.8% and 9.4%, respectively, compared to PID control.

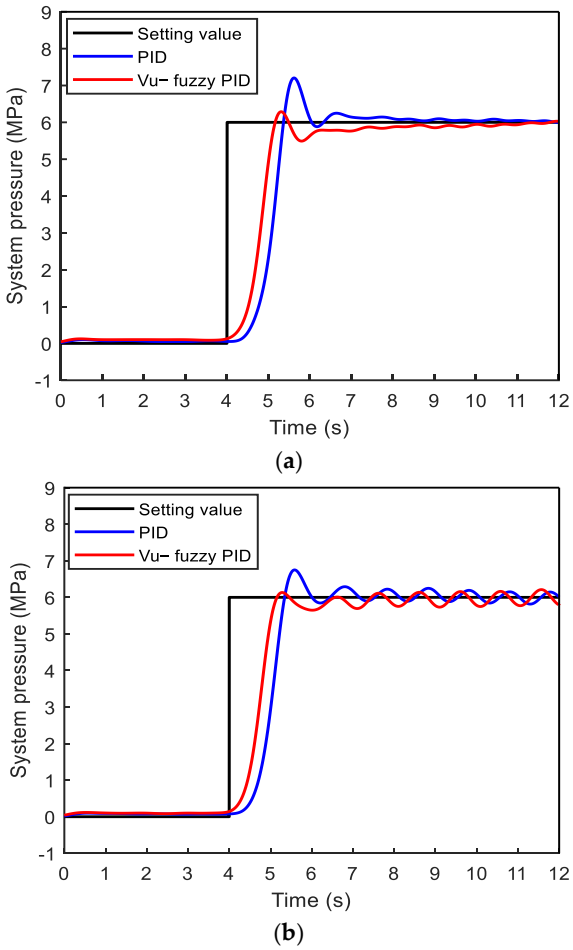
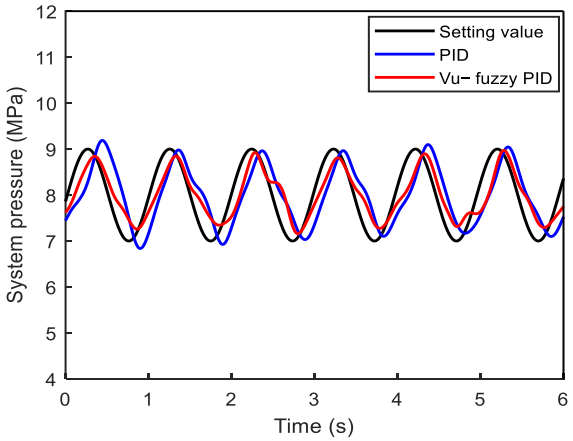


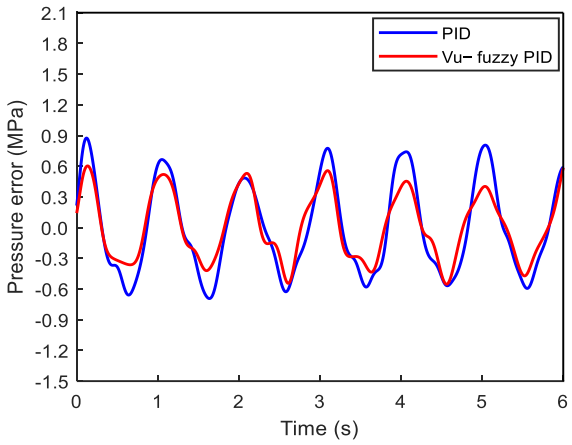
Figure 7. Simulation of 6 MPa Constant System Pressure. (**a**) Pressure Tracking Performance Under a Disturbance Signal of 3.4 ± 0.1 mA at 1.5 Hz. (**b**) Pressure Tracking Performance Under a Disturbance Signal of 3.4 ± 0.2 mA at 1 Hz.

As shown in Figure 8, when the system pressure is set to a sinusoidal variation of 8 ± 1 MPa at 1 Hz, and the input current of the proportional directional valve is adjusted to 3.4 ± 0.2 mA with a 1 Hz sinusoidal signal as the system disturbance, the proposed control algorithm reduces the pressure error by 31.7% and improves the responsiveness by 32.2% compared to PID control. Therefore, the tracking performance of the proposed algorithm is superior to that of PID control.



(**a**) Pressure Tracking Performance

Figure 8. *Cont.*



(**b**) Pressure Error Variation

Figure 8. Simulation of 8 ± 1 MPa, 1 Hz Sine Wave System Pressure.

4.2. Experimental Validation

To verify the responsiveness and anti-interference performance of the proposed algorithm, experiments were conducted on the dynamic source test platform under different system pressure values using the proposed algorithm. Simultaneously, the input signal of the proportional directional valve was adjusted as the disturbance value. The experimental results of the proposed algorithm were compared with those of PID control. As shown in Figure 9, the test platform mainly consists of an asynchronous servo motor, a variable displacement pump, a pressure sensor, a relief valve, a three-position four-way proportional directional valve, a Speedgoat controller, a servo drive controller, and an upper computer. The Speedgoat board model is IO133, and the servo drive control unit is CU310-2 PN, which communicate in real time via an Ethernet cable. Since the Speedgoat control terminal uses voltage inputs and outputs, an isolation module for current-to-voltage conversion is required for the pressure sensor. The specific parameters of the test platform are shown in Table 5.

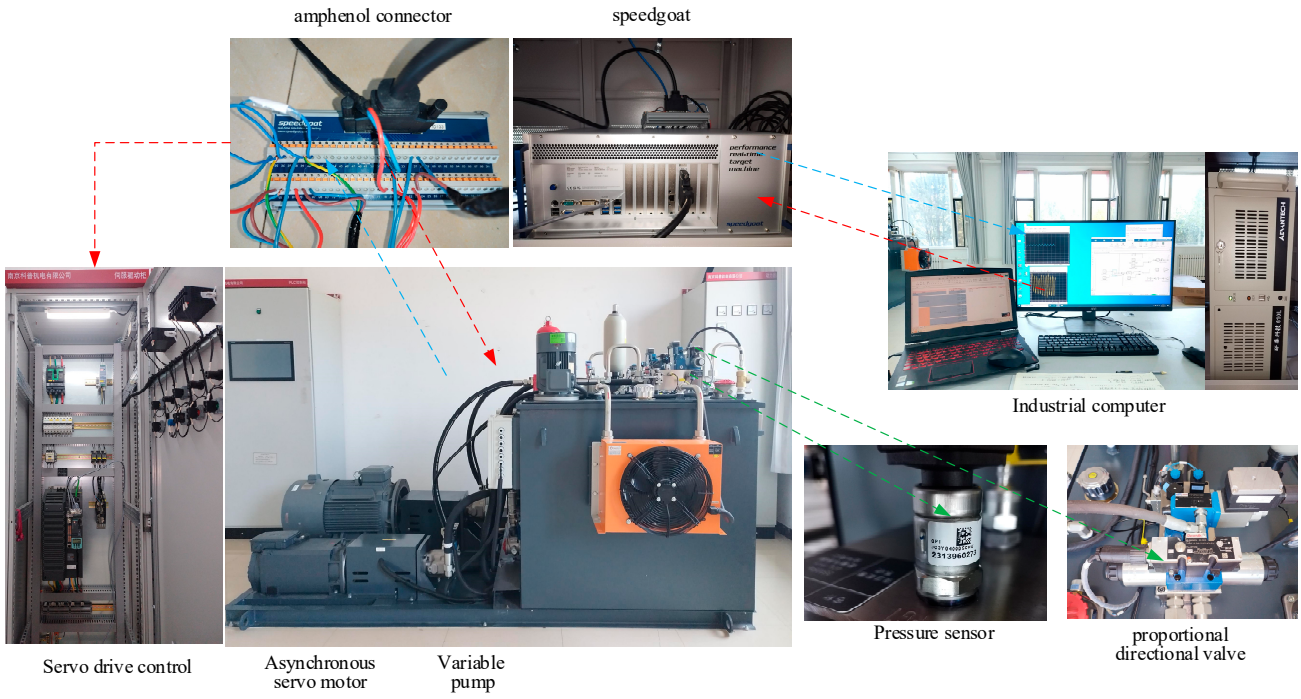


Figure 9. Test Rig Photograph.

Table 5. Components of the Test Platform.

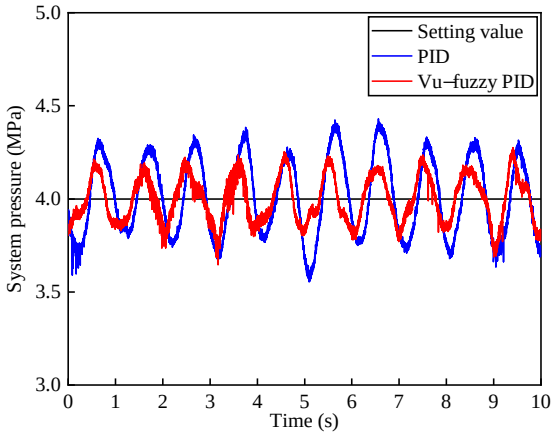
Element	Type	Signal
Electric Motor	1PH8137-1HG03-2BA2	Input 0–10 V
Variable Pump	SYDFEE-20/028R-PPA12N00	Input 0–10 V
Proportional Directional Valve	4WRAE10E60-22/G24K31/F1V	Input ±10 V
Pilot Operated Relief Valve	DBEE10-30/315YG24Z31/F1	Input 0–10 V
Pressure Sensor	Honeywell GPTJG3YG400BSCHX ± 0.5%FSS	Output 4–20 mA

4.3. Discussion of Experimental Results

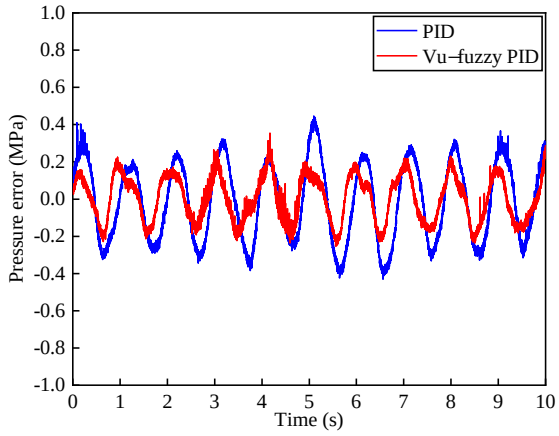
The experimental results provide a comparison of the performance of the two controllers under different system pressure setpoints.

(1) Constant Value

The system pressure was set to 4 MPa, with the voltage value of the three-position four-way proportional directional valve set to 3.4 ± 0.1 V and a frequency of 1 Hz. The system pressure performance under the two control algorithms is shown in Figure 10. From Figure 10a, it can be observed that although both controllers maintain the system pressure around 4 MPa, the pressure fluctuation of the proposed algorithm is smaller compared to PID control. As shown in Figure 10b, the proposed method reduces the pressure tracking error by approximately 36.5%.



(**a**) Pressure Tracking Performance



(**b**) Pressure Error Variation

Figure 10. 4 MPa Constant System Pressure Test.

(2) Step Value

To investigate the step response of the system pressure under the two algorithms, the initial pressure was set to 0 MPa, stepping to 6 MPa after 4 s, as shown in Figure 11.

In Figure 11a, the voltage of the three-position four-way proportional directional valve was set to 3.4 ± 0.1 V with a frequency of 1.5 Hz, while in Figure 11b, the voltage was set to 3.4 ± 0.2 V with a frequency of 1 Hz. From both Figure 11a,b, it can be observed that compared to PID control, the proposed algorithm reduces the response time by 6.8% and 8.2%, respectively, and decreases the overshoot by 16.2% and 10.3%, respectively. The steady-state error is approximately the same for both algorithms, around 0.4 MPa. Comparing Figure 11b with Figure 11a, it can be seen that as the disturbance frequency and valve opening increase, the overall pressure fluctuation under both control algorithms becomes larger, approximately 0.65 MPa.

(3) Sine Value

To investigate the tracking performance of the two algorithms under identical disturbances, the system pressure was set to a sinusoidal input signal of 8 ± 1 MPa with a frequency of 1 Hz, while the voltage of the proportional directional valve was adjusted to 3.4 ± 0.2 V at the same frequency. As shown in Figure 12, compared to PID control, the proposed algorithm reduces the system pressure tracking response time by 31.6% and decreases the pressure error by approximately 29.4%.

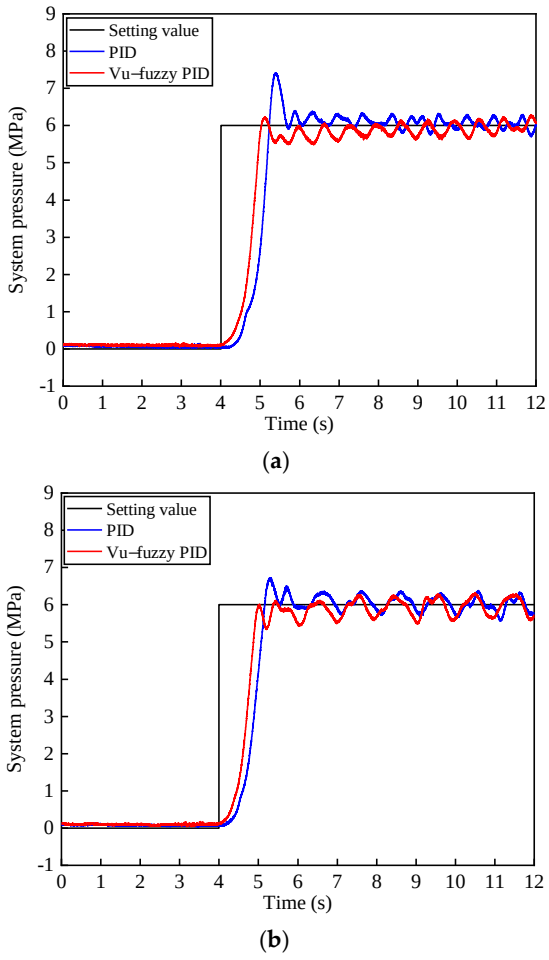
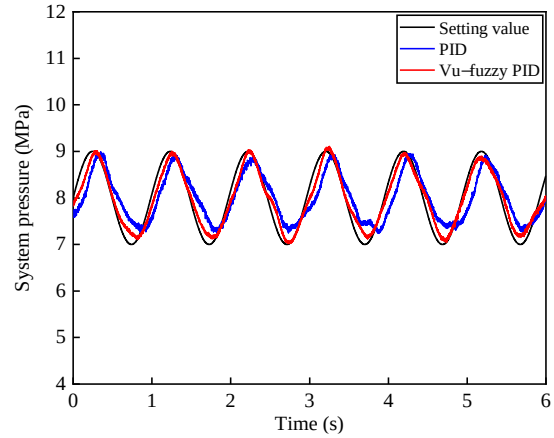
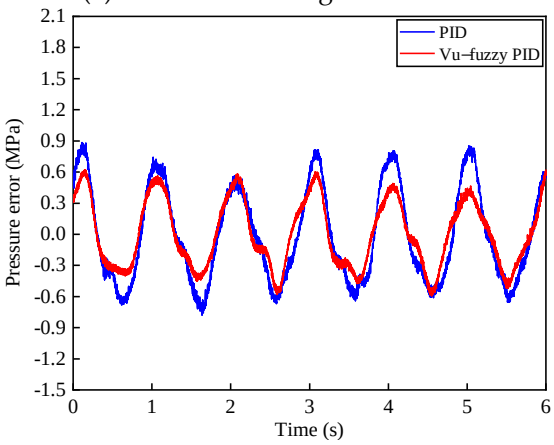


Figure 11. 6 MPa Step System Pressure Test. (**a**) Pressure Tracking Performance Under a Disturbance Signal of 3.4 ± 0.1 V at 1.5 Hz. (**b**) Pressure Tracking Performance Under a Disturbance Signal of 3.4 ± 0.2 V at 1 Hz.



(**a**) Pressure Tracking Performance

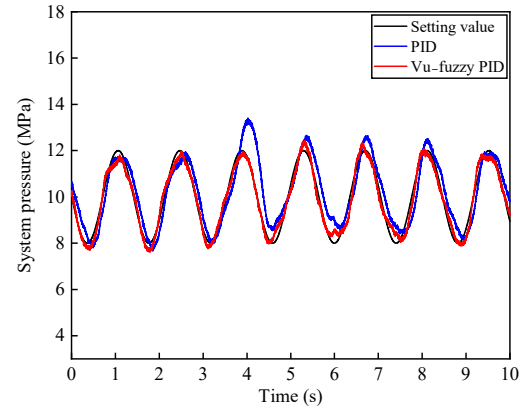


(**b**) Pressure Error Variation

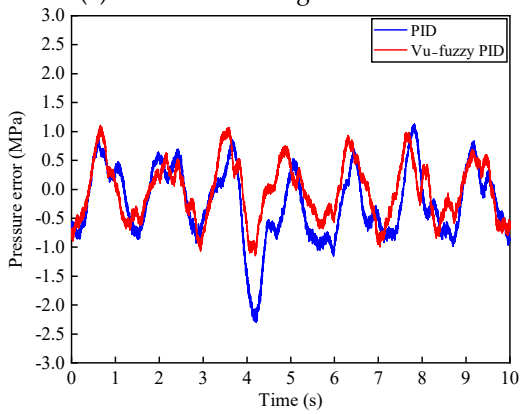
Figure 12. 8 ± 1 MPa, 1 Hz Sine Wave System Pressure Test.

To further investigate the tracking performance of the pump-controlled system pressure under abrupt disturbance changes, the system pressure was set to a sinusoidal input signal of 10 ± 2 MPa with a frequency of 0.7 Hz. The initial voltage of the three-position four-way proportional directional valve was set to 3.3 ± 0.1 V with a frequency of 0.5 Hz, and at 3.8 s, the voltage was adjusted to 3.3 ± 0.1 V with a frequency of 1.5 Hz. The system pressure tracking performance is shown in Figure 13. From the figure, it can be observed that during the first 3.8 s, the proposed algorithm demonstrates better responsiveness compared to PID control, with both algorithms exhibiting similar pressure error values. After the disturbance frequency increases, PID control shows an overshoot of nearly 2.5 MPa, taking approximately 1.1 s to stabilize, while the proposed algorithm remains almost unaffected. This demonstrates that the proposed algorithm has superior anti-interference performance compared to PID control.

Under the same sinusoidal input signal of 10 ± 2 MPa with a frequency of 0.7 Hz for the system pressure, the voltage of the three-position four-way proportional directional valve was initially set to 3.3 ± 0.1 V with a frequency of 1.5 Hz. After 4 s, the voltage was adjusted to 3.5 ± 0.1 V while maintaining the same frequency of 1.5 Hz. The system pressure tracking performance is shown in Figure 14. From Figure 14a, it can be observed that during the first 4 s, both control algorithms exhibit similar tracking performance for the sinusoidal pressure signal. However, after increasing the voltage bias of the proportional directional valve, PID control shows a significant overshoot of approximately 3 MPa, taking 2.2 s to stabilize, while the proposed algorithm exhibits only minor pressure fluctuations.

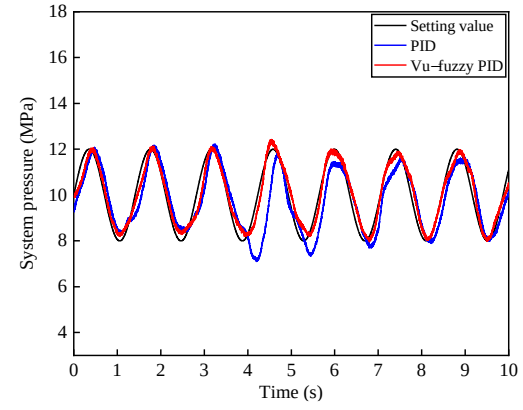


(**a**) Pressure Tracking Performance

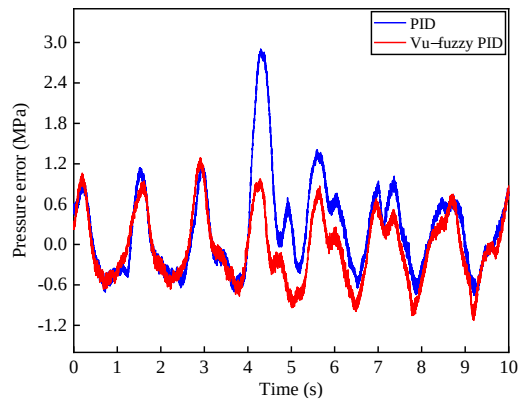


(**b**) Pressure Error Variation

Figure 13. Sine Wave System Pressure Test Under Disturbance Frequency Variation.



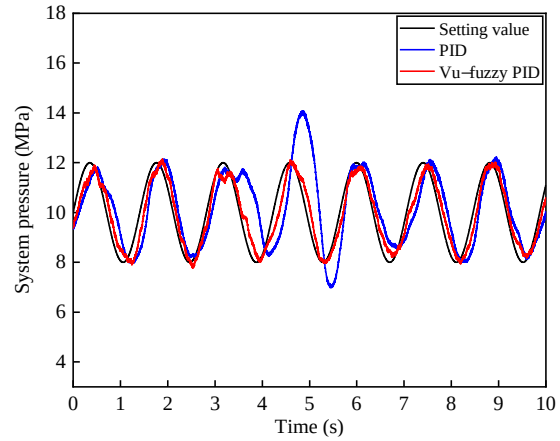
(**a**) Pressure Tracking Performance



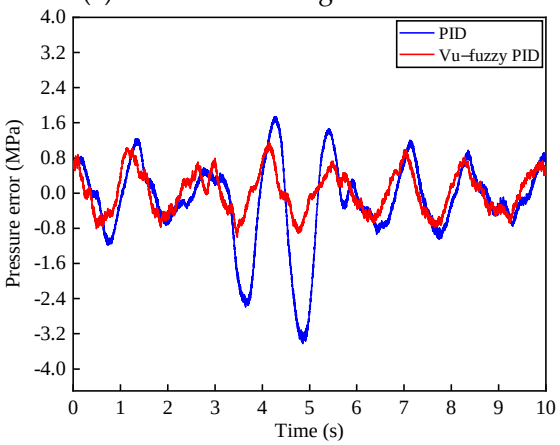
(**b**) Pressure Error Variation

Figure 14. Sine Wave System Pressure Test Under Disturbance Offset Variation.

Under the same sinusoidal input signal of 10 ± 2 MPa with a frequency of 0.7 Hz for the system pressure, the voltage of the three-position four-way proportional directional valve was initially set to 3.45 ± 0.1 V with a frequency of 1 Hz. After 3 s, the voltage was switched to 3.45 ± 0.2 V while maintaining the same frequency of 1 Hz. The system pressure tracking performance is shown in Figure 15. From the figure, it can be observed that in the first 3 s, the proposed control algorithm reduces the response time by 6.2% and decreases the pressure error by approximately 15.4% compared to PID control. As the amplitude of the proportional directional valve's voltage increases, resulting in a further expansion of the valve's opening, both algorithms experience pressure fluctuations. However, PID control exhibits a larger overshoot and takes 2.8 s to resume tracking the system pressure. Therefore, the anti-interference performance and responsiveness of the proposed control algorithm are superior to those of PID control.



(**a**) Pressure Tracking Performance



(**b**) Pressure Error Variation

Figure 15. Sine Wave System Pressure Test Under Disturbance Amplitude Variation.

5. Conclusions

(1) This paper addresses the issue of significant system pressure fluctuations encountered during drilling operations of bolting rigs under complex surrounding rock conditions. A variable universe fuzzy PID method for pump-controlled system pressure is proposed. This method takes the output pressure of the fixed displacement pump as the controlled object and uses the variable universe fuzzy PID approach to regulate the motor speed, thereby indirectly adjusting the system pressure to achieve closed-loop pressure control.

(2) Based on the potential variations in the surrounding coal-rock conditions during the operation of the bolting rig, three system pressure scenarios were defined: constant pressure, step pressure, and sinusoidal pressure. By adjusting the opening of the three-

position four-way proportional directional valve as a system disturbance, the tracking performance of the two control algorithms was compared. From the paper, it can be seen that the proposed control method in the simulation model and the test conditions of the results are basically consistent, the effect of the reduced system pressure fluctuations is better than the PID control.

(3) Under the test, when the set pressure is a constant value of 4 MPa, the proposed algorithm can reduce the pressure error by about 36.5% compared to PID control; when the pressure is a step value of 0–6 MPa, the proposed algorithm's response time can be shortened by more than 6.8%, and its overshoot can be reduced by more than 10.3%; when the pressure is a sinusoidal value of 8 ± 1 MPa with a frequency of 1 Hz, the proposed control algorithm can reduce the pressure error by 29.4% and improve the responsiveness by 31.6% compared to PID control; when the pressure is 8 ± 1 MPa and the frequency is 1 Hz sinusoidal value, the proposed control algorithm reduces 29.4% of the pressure error and improves 31.6% of the responsiveness compared to PID control; when the pressure is 10 ± 2 MPa and the frequency is 0.7 Hz sinusoidal value, the proposed control algorithm has less influence when the frequency of the perturbed sinusoidal signal of the adjusting directional valve changes suddenly, and there is an overshooting amount of 2.5 MPa after perturbation in PID control; when the pressure is 10 ± 2 MPa and the frequency is 0.7 Hz sinusoidal value, when the disturbed sinusoidal signal bias of the regulating directional valve suddenly changes, the PID control is restored to stability after 2.2 s, while the proposed control algorithm has a shorter stabilization time; when the pressure is 10 ± 2 MPa, the frequency is 0.7 Hz sinusoidal value, when the disturbed sinusoidal signal amplitude of the regulating directional valve changes suddenly, the two control algorithms have pressure overshooting, but the proposed control algorithm amplitude of pressure fluctuation is smaller. From this, it can be concluded that the tracking effect of the proposed algorithm is better, and its anti-interference ability is stronger.

(4) The proposed algorithm provides a theoretical method for reducing pressure fluctuations in the intelligent control system of bolting rigs during operation. There are also some challenges: if the set system pressure changes too much, using the pump control method may lead to a larger motor speed adjustment, generating a larger noise, and even affecting the performance of the motor. The pump control system can reduce the system energy consumption and lower heat generation compared to the valve control system, and later research can use this control algorithm to conduct an in-depth study on the effect in the pump control and valve control systems, respectively, as well as the system's system low pressure and high pressure tracking effect. It can even focus on the design of controllers with fewer parameters and better control effects.

Author Contributions: Conceptualization, Z.Y.; methodology, G.T.; software, Y.G.; validation, Z.Y. and Y.G.; formal analysis, Y.G.; investigation, G.T.; resources, Z.Y.; data curation, G.T.; writing—original draft preparation, Z.Y. and G.T.; writing—review and editing, Z.Y. and G.T.; visualization, Y.G.; supervision, G.T.; project administration, Z.Y.; funding acquisition, Z.Y. All authors have read and agreed to the published version of the manuscript.

Funding: This research received Shanxi Provincial Department of Science and Technology, Central Guiding Local Science and Technology Development Fund Project, Fund No.: YDZJSX2022C030.

Data Availability Statement: Data are contained within the article.

Conflicts of Interest: The authors declare no conflicts of interest.

References

1. Kang, H.; Jiang, P.; Liu, C.; Wang, Z.; Luo, C.; Guo, J.; Chen, Z.; Cao, X. Current Status and Development Trends of Bolting Support Equipment in Coal Roadways. *Ind. Min. Autom.* **2023**, *49*, 1–18. [CrossRef]

2. Ren, Z.; Mao, J.; Xie, M.; Zhang, H.; Lu, J.; Li, Y.; Liu, Z. Analysis of Vibration Characteristics of a New Anchoring Drilling Rig System under Complex Conditions. *J. China Coal Soc.* **2023**, *48*, 3947–3958. [CrossRef]
3. Zhang, N.; Zhang, Y.; Shao, J.; Kan, Z. Research on the Hydraulic System of Double Power Heads in Anchor Drilling Rig. *IOP0020Conf. Ser. Earth Environ. Sci.* **2019**, *242*, 032024. [CrossRef]
4. Guo, C. Analysis of pressure regulating characteristics of safety valve in hydraulic system of offshore oil production equipment. *Ain Shams Eng. J.* **2022**, *13*, 101738. [CrossRef]
5. Cao, C.; Zhao, J.; Gao, K.; Wang, H.; Li, R.; Liu, H.; Zhang, H. Research on Rapid Pump-Controlled Liquid Replenishment and Pressure Stabilization Method for Hydraulic Support Liquid Supply System. *Coal Sci. Technol.* **2024**, 1–12. Available online: http://kns.cnki.net/kcms/detail/11.2402.TD.20240613.1528.007.html (accessed on 21 February 2025).
6. Cheng, M.; Hou, Y.; Ding, R. A Nonlinear Filtering Method of Vibration Suppression for the Independent Metering Control System. *J. Xi'an Jiaotong Univ.* **2024**, *58*, 200–211. [CrossRef]
7. Chen, Y.; Chen, C.; Peng, Z.; Chen, H.; Wng, M.; Shi, H. Study on the Influence of Accumulator Parameters on Hydraulic Impact in Cane Cutting and Segmentation Load-Sensitive Systems. *J. Vib. Shock* **2023**, *42*, 270–277. [CrossRef]
8. Wei, L.; Liu, Y.; Wang, X.; Liu, Z.; Li, L. Pressure Control Strategy for a Steer-by-Wire Braking System Based on Hierarchical Control. *J. Mech. Eng.* **2024**, *60*, 487–496. [CrossRef]
9. Zhang, Y.; Du, Y.; Meng, Q.; Li, X.; Liu, L.; Zhu, Z. Adaptive Pressure Control of Wet Clutches Based on an Improved Genetic Algorithm. *J. Jilin Univ.* **2024**, *54*, 852–864. [CrossRef]
10. Gao, Q.; Li, L.; Zhu, Y. Hybrid Coding Control of Array Digital Valve-Controlled Electro-Hydraulic Pressure Servo System. *J. Mech. Eng.* **2024**, *60*, 143–154. [CrossRef]
11. Chen, Z.; Lü, L.; Wang, F.; Yao, B.; Li, D.; Liu, H.; Zhang, G. Motion Control of Load-Independent Electro-Hydraulic Systems Based on Chamber Pressure Planning Without Mode Switching. *J. Mech. Eng.* **2024**, *60*, 302–312. [CrossRef]
12. Su, C.; Wang, C.; Yuan, Y.; Zhao, E.; Quan, L.; Cheng, L. Active Disturbance Rejection Control Method for Valve-Controlled Electro-Hydraulic Servo Pressure Pulse Experiment. *Control Decis.* **2024**, *39*, 1927–1935. [CrossRef]
13. Ge, L.; Yang, F.; Quan, L.; Zhang, H.; Yan, Z. Operating Characteristics of a Constant Pressure Electro-Hydraulic Power Source with Fixed Displacement Based on Torque Control. *J. Mech. Eng.* **2022**, *58*, 453–460. [CrossRef]
14. Li, W.; Gong, G.; Liu, J.; Zhang, Y.; Yang, H. Simulation of Train Brake Electro-Hydraulic System Based on High-Frequency Solenoid Valve Pressure Control. *J. Cent. South Univ. (Sci. Technol.)* **2020**, *51*, 340–348. [CrossRef]
15. Tan, C.; Yu, P.; Li, B.; Lu, J.; Ren, Y. Pressure Cascade Control of a Direct-Drive Pump-Valve Coordinated Steer-by-Wire Braking Unit. *J. Beihang Univ.* **2024**, 1–13. [CrossRef]
16. Xia, Y.; Luo, L.; Guo, K.; Yuan, Y.; Shi, Y.; Wang, C. Pressure-Velocity Compound Control Strategy for Hydraulic Systems. *J. South China Univ. Technol.* **2023**, *51*, 31–40. [CrossRef]
17. Zhong, Q.; Zhang, B.; Bao, H.-M.; Hong, H.-C.; Ma, J.-E.; Ren, Y.; Yang, H.-Y.; Fung, R.-F. Analysis of pressure and flow compound control characteristics of an independent metering hydraulic system based on a two-level fuzzy controller. *J. Zhejiang Univ.-Sci. A* **2019**, *20*, 184–200. [CrossRef]
18. Feng, J.; Gao, Q.; Shao, Y.; Qian, W. Research on Flow-Pressure Compound Control Strategy for Missile Hydraulic Erection System. *Acta Armamentarii* **2018**, *39*, 209–216. [CrossRef]
19. Yu, J.; Chen, H.; Liu, J. Variable Universe Fuzzy PID Ratio Tracking Control of Hydraulic Mechanical Continuously Variable Transmission. *China Mech. Eng.* **2019**, *30*, 1226–1232. [CrossRef]
20. Gao, Y.; Cheng, J.; Huang, J.; Quan, L. Simulation Analysis and Experiment of Variable Displacement Asymmetric Axial Piston Pump Characteristics. *J. Mech. Eng.* **2018**, *54*, 215–224. [CrossRef]
21. Lyu, D.C.; Zhao, S.J.; Zeng, S.; Fu, J.; Hu, X.; Liu, H.; Miao, K.; Fu, Y. Key technologies and challenges of high-performance servo-motor-pumps. *Acta Aeronaut. Astronaut. Sin.* **2024**, *45*, 630225. (In Chinese) [CrossRef]
22. Yan, Z. Characteristics of high energy-efficient Electro-hydraulic power source driven by servo motor and variable pump. *Proc. Inst. Mech. Eng. Part C J. Mech. Eng. Sci.* **2023**, *237*, 1525–1536. [CrossRef]
23. Abdul Ali, A.W.; Abdul Razak, F.A.; Hayima, N. A Review on The AC Servo Motor Control Systems. *ELEKTRIKA-J. Electr. Eng.* **2020**, *19*, 22–39. [CrossRef]
24. Pan, X. Research on AC Asynchronous Servo Control System Based on MTPA. Master's Thesis, Harbin University of Science and Technology, Harbin, China, 2023.
25. Cao, Z.; Zheng, S. MR-SAS and electric power steering variable universe fuzzy PID integrated control. *Neural Comput. Appl.* **2019**, *31*, 1249–1258. [CrossRef]
26. Zhang, X.; Kang, L.; Tang, J.; Zhang, J. Trajectory Tracking of Intelligent Excavators Based on Variable Universe Fuzzy Multi-Parameter Self-Tuning PID Control. *China J. Highw. Transp.* **2023**, *36*, 240–250. [CrossRef]
27. Ge, L.; Ni, H.; Hao, Y.; Zhao, B.; Yuan, Y.; Quan, L. Dead Zone Compensation Control for a Novel Hydraulic Rotary-Mechanical Linear Actuator. *J. Mech. Eng.* **2024**, *60*, 337–347. [CrossRef]

28. Ji, G.; Zhang, L.; Cai, M.; Meng, X.; Du, Z.; Ruan, J.; Guan, S.; Liu, Z. Research on variable universe fuzzy PID control for semi-active suspension with CDC dampers based on dynamic adjustment functions. *Sci. Rep.* **2024**, *14*, 3442. [CrossRef]
29. You, X.; Guo, Y.; Miao, B.; Ge, S. A Digital Twin-Based Adaptive Height Control for a Shearer. *Machines* **2024**, *12*, 460. [CrossRef]
30. He, J.; Su, S.; Wang, H.; Chen, F.; Yin, B. Online PID Tuning Strategy for Hydraulic Servo Control Systems via SAC-Based Deep Reinforcement Learning. *Machines* **2023**, *11*, 593. [CrossRef]

Disclaimer/Publisher's Note: The statements, opinions and data contained in all publications are solely those of the individual author(s) and contributor(s) and not of MDPI and/or the editor(s). MDPI and/or the editor(s) disclaim responsibility for any injury to people or property resulting from any ideas, methods, instructions or products referred to in the content.